

MODELLING OF LITHIUM ION BATTERY

Nagendra Thogaru¹, Mahender Kodela ²

¹ M.Tech scholar, Department of EEE, Vaagdevi college of Engineering (Autonomous), Warangal,

²Assistant Professor, Department of EEE, Vaagdevi college of Engineering (Autonomous), Warangal.

Abstract - This paper presents an optimal control-based energy management strategy for a parallel hybrid electric vehicle (HEV). Not only does this strategy try to minimize fuel consumption while maintaining the state of charge of the battery within reasonable bounds, it also seeks to minimize wear of the battery and extend its life. This paper focuses on understanding the optimal control solution offered by Pontryagin’s minimum principle (PMP) in this context. Simulation-based results are presented and analyzed, which show that the control algorithm is able to reduce battery wear by decreasing battery operating severity factor with minimal fuel economy penalty. The benefit of this strategy is especially evident when ambient and driving conditions are especially severe.

Key Words: Battery aging, energy management, hybrid electric vehicle (HEVs), optimal control, Pontryagin’s minimum principle (PMP).

1.INTRODUCTION

Rechargeable battery is an electrochemical device which converts electrical energy to chemical energy during charging and converts chemical energy to electrical energy during discharging. Rechargeable battery plays important role in future technology since it is potentially to be applied as energystorage element in green technology applications, such as electric vehicle (EV) and photovoltaic (PV) system. The renewable energy source can be stored in battery packs and thus help to reduce the reliance on fossil fuels.

In the aspect of technology, the rechargeable battery is improved from lead acid battery to nickel-based battery and from nickel-based battery to lithium-ion (Li-ion) battery. Lithium-ion battery has higher terminal voltage, higher power density and higher energy density compared to the other rechargeable batteries. Nowadays, Li-ion battery is widely adopted in portable electronic devices, such as laptop computers, smart phones and digital cameras.

Accurate battery information such as state-of-charge (SOC), current and voltage are vital for circuit designer to manage the energy consumption of battery-powered system. Moreover, handling on battery is necessary to avoid battery from overcharged or over-discharged. Therefore, an accurate battery model is vital as a guide in circuit design process to forecast the characteristics of battery.

Numerous studies conducted on battery modeling techniques are published in various scientific journals.

Equivalent circuit model is popularly used by circuit designers since it can be easily applied in circuit simulator [1-2]. Reference [1] has proposed an accurate and intuitive equivalentcircuit model for battery as shown in Fig. 1. This battery model with two resistor-capacitor (RC) parallel networks is proven to have high accuracy and capable to predict runtime and current- voltage (I-V) performance of

battery [1].

battery model is included in MATLAB/Simulink SimPowerSystems library as proposed in [3]. However, the model is built based on Sheperd equation, is not capable to characterize the nonlinear current-voltage performance of battery [4]. Therefore, a new battery model which based on equivalent circuit model should be developed in MATLAB/Simulink in order to give a more accurate simulation results. For instance, a Simulink model of Li-ion battery has been developed in [5] using Simulink blocks. Average values of RC circuit parameter are applied in the Simulink model for model simplification.

In this paper, an equivalent circuit model for battery is developed in MATLAB/Simulink. The parameters of battery model are determined from experiment results. In contrast to the model proposed in [5], the model’s parameters are varied with state-of-charge (SOC) and current [1,6] and it allows circuit designer to set the parameters according to the battery behaviors. Moreover, the proposed model can be easily connected to another circuit blocks in MATLAB/Simulink and give real time SOC estimation.

The rest of paper is organized as follow. Section II introduces the proposed model and explains the structure of simulation blocks. Battery test system and model extraction are

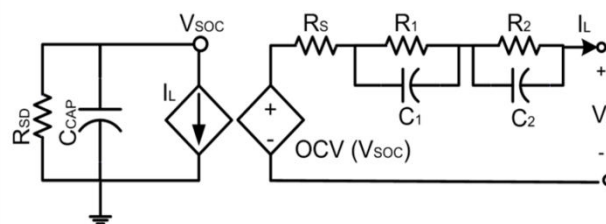


Fig. 1. Equivalent circuit model in [1].

2. FORECASTING OF SOLAR INSOLATION AND LOAD DEMAND

In a conventional utility grid, load forecasting is done for supply and load power balancing and power system planning. But in the case of a smart grid, the effect of distributed energy resources (DER) like solar must be considered. The power generated by these DERs is highly intermittent in nature. Hence proper forecasting tools must be employed for short term load and PV power forecasting to ensure continuity of power to the connected loads. In this project these forecasted variables are used to determine the charging and discharging half cycle times of the battery. These variables are then used to determine the battery power at each time instant such that the degradation cost of battery is minimized.

2.1 Description of the Methodologies Used

2.1.1 Artificial Neural Networks

These are biologically inspired networks which consists of connected nodes. The connection is similar to synapse in a biological neuron which transmits the information from one neuron to other. The schematic diagram of a neural network is given in figure 2.1. The neural network consists of weights and biases and each node has a non-linear activation function. A deep neural network consists of an input layer, hidden layers and an output layer. The number of nodes in the input and the output layers will be equal to the number of input and output variables respectively. But the number of hidden layers and their nodes will vary from problem to problem. They are generally chosen by trial and error method or by using some tuning methods.

The neural networks can be trained using supervised learning technique where the network is supplied with input and target variables. The network is trained in an iterative manner using back propagation algorithm in which its weights and biases are adjusted to approximate the non-linear relationship between the input and output variables. A loss function is chosen and it is minimised in subsequent iterations. These iterations in training are termed as epochs.

Apart from conventional feedforward neural network (FFNN), there is long short term memory network (LSTM) which is a type of recurrent neural network. These are mostly used for sequential data processing. An LSTM node contains a memory cell which remembers values for certain number of time intervals and it also has three gates (input gate, output gate and forget gate) in it. These gates regulate the flow of information into and out of the cell. In time series forecasting these LSTMs are used to model time dependencies between successive time steps.

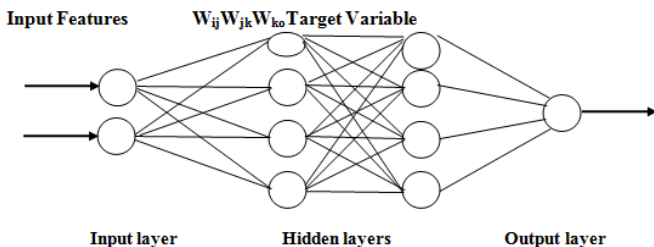


Figure 2.1 Schematic Diagram of a Neural Network

2.1.2 Random Forest Regression

Random Forest Regression is a type of ensemble learning algorithm in which number of regression trees are trained using same dataset and while predicting, the average of predictions is taken as the output. The trees are trained by a technique known as bagging in which the available dataset is sampled with replacement [20].

The main advantage of ensemble learning method is that as we are training different models using same data, it results in reduced variance in the predictions compared to a single model.

2.3 Implementation of Forecasting

2.3.1 Inputs Used For Forecasting

While choosing the input variables, pearson correlation coefficient (PCC) between the input variable and the output variable is evaluated and the variables having PCC near to 1 or -1 are selected. The insolation is highly correlated with humidity and load demand has good correlation with

previous day load at the same hour. The inputs used for insolation and load forecasting are given in table 2.2.

Table 2.2 Inputs Used For Insolation and Load Forecasting

Inputs for solar insolation forecasting	Inputs for load forecasting
<ul style="list-style-type: none"> • Time of day (hrs) • Temperature (⁰C) • Relative humidity (%) • Cloud data • Wind speed(m/s) 	<ul style="list-style-type: none"> • Time of day (hrs) • Temperature(⁰C) • Month (1-12) • Day of week (1-7) • Previous day load at the same hour(W)

2.3.2 Performance Metrics

2.3.2.1 Mean Absolute Error

Mean absolute error (MAE) is the mean of magnitudes of errors in a set of output samples (2.1). In this metric equal weights are given to all the errors irrespective of their magnitudes.

$$MAE = \frac{1}{N} \sum_{j=1}^N |T_j - F_j| \tag{2.1}$$

Where T_j is the true value and F_j is the forecasted value. Here N is the number of samples.

2.3.2.2 Root Mean Squared Error

Root Mean Squared Error (RMSE) is the square root of average of squared errors (2.2). RMSE gives relatively more weightage to large errors in the output samples.

$$RMSE = \sqrt{\frac{1}{N} \sum_{j=1}^N |T_j - F_j|^2} \tag{2.2}$$

2.3.2.3 Mean Absolute Percentage Error

Mean Absolute Percentage Error (MAPE) is the average of absolute errors expressed with respect to true value (2.3). It can be expressed as a percentage by multiplying with 100.

$$MAPE = \frac{1}{N} \sum_{j=1}^N \left| \frac{T_j - F_j}{T_j} \right| \times 100 \tag{2.3}$$

2.3.2.4 Coefficient of Determination

The coefficient of determination (R₂_score) represents the variance in the dependent variable that can be predicted from the independent variable.

2.3.3 Procedure

The forecasting models are implemented in python 3.7.4 jupyter notebook software using tensorflow and keras APIs. For ANNs the input features are scaled between the range 0 and 1 and this data is splitted into training and testing sets. Two hidden layers are used and the number of neurons in these

layers are decided based on hyper parameter tuning. In this tuning process, the minimum and maximum values of neurons must be specified and the best number of neurons are identified using grid search technique [21]. The network architectures are given in tables 2.3 and 2.4.

For inputs to ANNs with LSTM layer, the inputs are prepared in the form of a two dimensional array with different time steps. The activation function used for hidden layers is Relu and for output layer is linear. The optimizer used is adam and the loss function is MAE. While training, early stopping technique is used to avoid overfitting of the model. This would stop the training process when the validation loss is almost constant for a certain preset number of epochs.

Table 2.3 Network Architectures for Insolation Forecasting

Parameter	FFN N	LSTM
No. of hidden layers	2 (Dense)	2 (LSTM, Dense)
No. of neurons in the 1 st layer	84	44
No. of neurons in the 2 nd layer	28	52
No. of neurons in the output layer	1	1
Max. no of epochs set	200	250
No. of epochs executed	48	62
No. of time steps in each input	-	3

Table 2.4 Network Architectures for Load Forecasting

Parameter	FFN N	LSTM
No. of hidden layers	2 (Dense)	2 (LSTM, Dense)
No. of neurons in the 1 st layer	86	85
No. of neurons in the 2 nd layer	62	90
No. of neurons in the output layer	1	1
Max. no of epochs set	250	250
No. of epochs executed	106	35
No. of time steps in each input	-	3

In the implementation of random forest regression, the scaling of input features is not required as in the case of ANNs. The number of trees used for training in insolation forecasting are 2000 and in load forecasting are 1000.

3. Results of Forecasting

3.1 Performance Metrics

The performance metrics evaluated for each forecasting method for both insolation and load forecasting are given in tables 3.3 and 3.4.

Table 3.5 Errors in Solar Insolation Forecasting

	MAE (W/m^2)	RMSE (W/m^2)	R2_s core
LSTM	27.67	68.916	0.933
FFNN	30.65	68.66	0.933
Random Forest	30.936	67.366	0.936

Table 3.6 Errors in Load Forecasting

	MAE (W)	RMS E (W)	MAP E (%)	R2_s core
LSTM	36.91	46.26	1.065	0.994
FFNN	129.3	173.6	3.541	0.921
Random Forest	132.1	180.1	3.617	0.922

From the above results, it is clear that in case of insolation forecasting, LSTM is showing somewhat better result when compared to other methods. In case of load forecasting also LSTM network is more accurate and the errors are vary less compared to other methods. The plots of true and forecasted values of different techniques are shown below in figures 2.2 to 2.7. We can observe from these plots also that forecasting with LSTM showed accurate results and the forecasted values closely follows the true value.

3.2 Plots Showing True Value and Forecasted Values

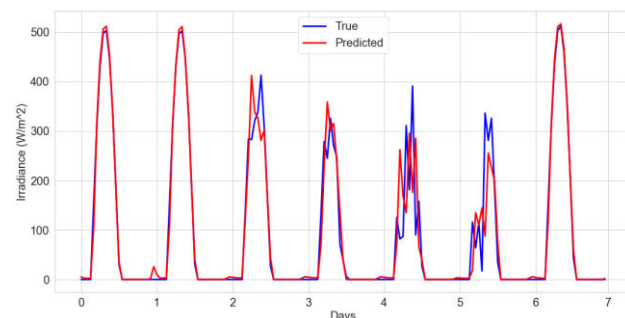


Figure 2.2 Insolation Forecasting Using LSTM Network

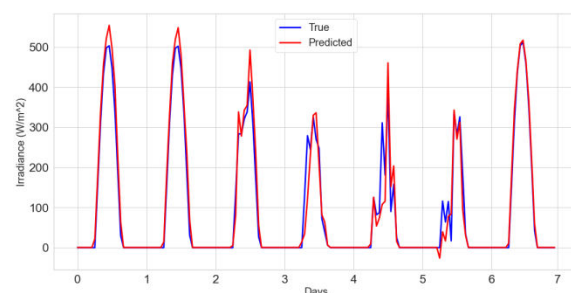


Figure 2.3 Insolation Forecasting Using FFNN

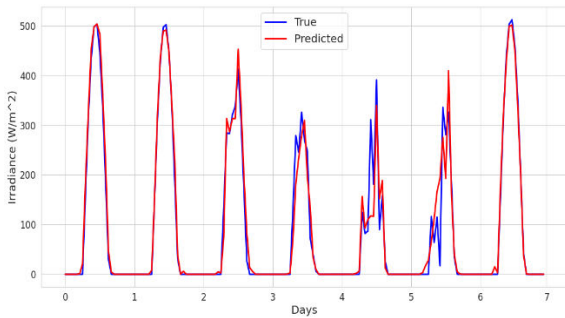


Figure 2.4 Insolation Forecasting Using Random Forest Regression

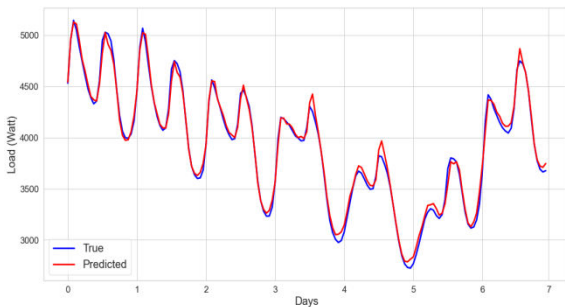


Figure 2.5 Load forecasting using LSTM

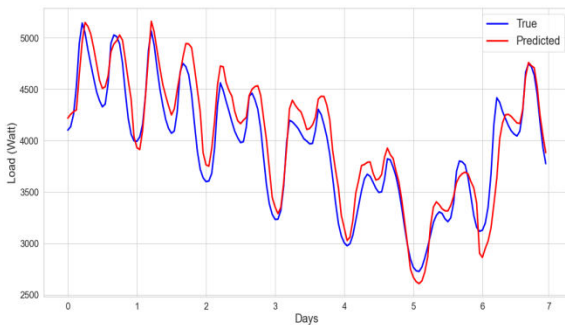


Figure 2.6 Load forecasting using FFNN

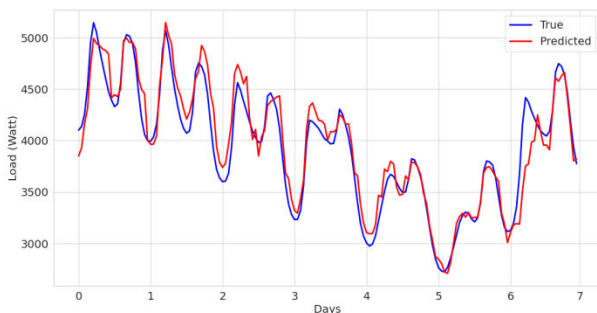


Figure 2.7 Load forecasting using Random Forest Regression

3. SYSTEM DESCRIPTION AND BATTERY AGEING MODEL

In this chapter, the system considered for this project is described with the help of a block diagram. The sizing of various components is explained along with their specifications and ratings. The operation of the system under normal and grid outage conditions is explained and the variations of battery and grid powers are shown by creating outages for different durations of time. The ageing model is

described along with the factors effecting the ageing of Li-ion battery. The severity factor of Li-ion battery is defined and its variation due to different factors is shown. An equation for the degradation cost of battery is derived using the effective Ah throughput.

3.1 Components in the System

3.1.1 Residential Load

The connected load in the system is assumed according to the load dataset. The dataset contains data of load demand of an utility. Hence in order to get only residential load demand from it, 24% of it is considered as residential and in that 50% is assumed as prosumers load demand. The maximum demand in the load dataset is 7397 W. Hence the connected load is assumed to be **10 KW** as the residential demand factor will be around 50% to 80% [22].

3.1.2 Rooftop PV Array

According to the rules and regulations in many states in India, the peak capacity or the rated capacity of rooftop PV array should not exceed the connected load of the connection [23]. Hence the size of PV array is fixed as **10 KW peak**. The specifications of the PV array are given in table 3.1.

Table 3.1 Specifications of PV Array

Parameter	Value
Nominal power of each panel	345 W
Panel efficiency	21.5 %
No. of panels	28
No. of panels in a string	14
No. of parallel strings	2
Area of the PV array	45.36 m ²

The area which the PV array occupies is assumed shadow free so that complete insolation is received by the panels.

3.1.3 Battery Energy Storage System

The size of the BESS is decided based on the critical load in the system. 20% of the connected load in the system is assumed as critical load and the battery pack is sized to meet the critical load demand approximately for 12 hrs in case of grid outage. The critical load demand in the system will be 2000 W which cannot be shedded and must be supplied power even in outage conditions. Hence twelve 12V, 180Ah, LiFepO4 batteries are employed to give a total capacity of **25.920 kWh**. These are connected in 4 series and 3 strings parallel configuration to form a 48V system.

3.1.4 Specifications of the System

The specifications of the system are given in the table 3.2 and the block diagram of the system is given in figure 3.1.

Table 3.2 Specifications of the System

Component	Rating
t	

Connected load	10 KW
Critical load	2 KW
PV array	10 KW peak
Energy storage	12V, 180 Ah, 12 batteries

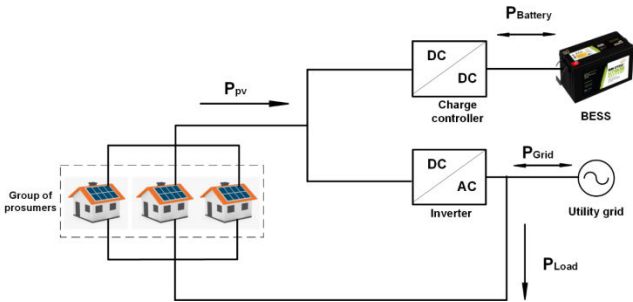


Figure 3.1 Block Diagram of the System

3.2 Operation of the System

When the solar insolation is sufficiently available, the PV array supports the load demand and charges the battery. When PV power generation is less, deficit of power arises in the system and this deficit is supplied by either BESS or grid. The battery and grid powers are decided by the optimization framework which is explained in the next sections. Under grid outage conditions, the BESS supports only the critical loads present in the system. The operation of the system under normal condition and grid outage condition is shown below in figures 3.2 to 3.8 by creating outages for different durations of time in a day.

In these figures as optimization is not performed, it is considered as 30 % of the deficit power is supplied by the BESS and remaining power is supplied by the grid and the initial SOC is assumed as 0.4.

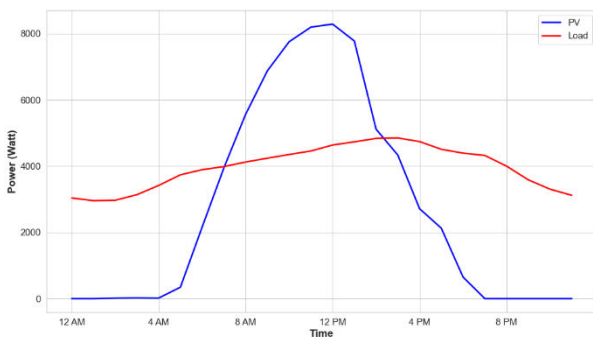


Figure 3.2 Variation of PV Power and Load Power

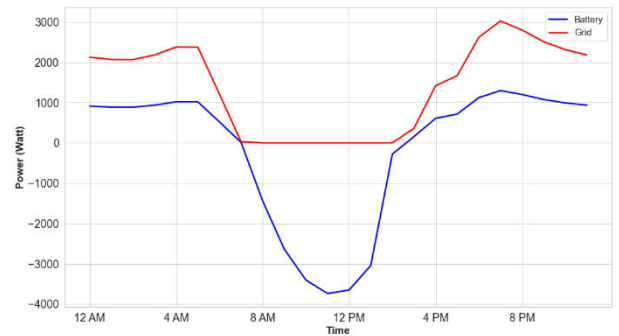


Figure 3.3 Variation of Battery and Grid powers under Normal Condition

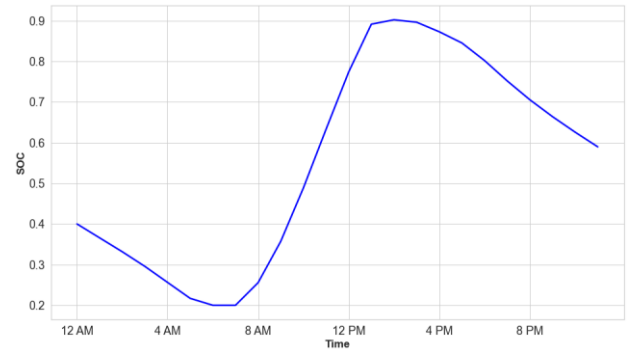


Figure 3.4 Variation of SOC Under Normal Condition

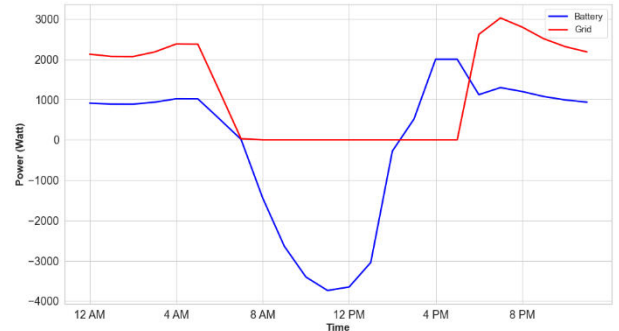


Figure 3.5 Variation of Battery and Grid Powers under Outage of 3 hrs

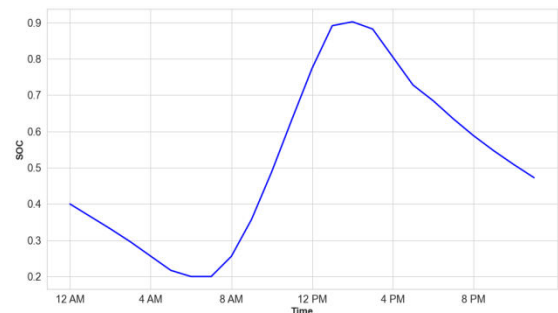


Figure 3.6 Variation of SOC under Outage of 3 hrs

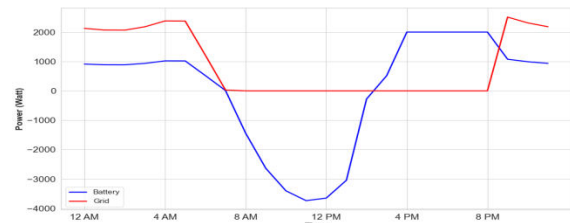


Figure 3.7 Variation of Battery and Grid Powers under Outage of 6 hrs

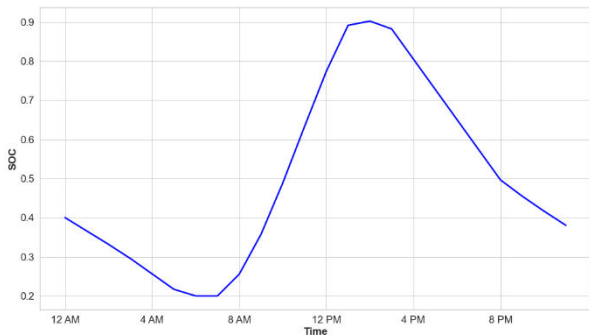


Figure 3.8 Variation of SOC under Outage of 6 hrs

3.3 Weighted Ah-throughput Models

The useful life of battery can be estimated by measuring number of cycles, weighted Ah throughput or effective Ah throughput (Ah_{eff}), time since installation etc. In this project, a weighted Ah throughput model in which the ageing is effected by temperature, state of charge and discharge rate (C-rate) of the battery is considered. The Ah_{eff} of a battery can be measured with the help of 3.1 [16].

$$Ah_{eff} = \sum_{k=1}^{N_i} W_E \cdot Ah_E \quad (3.1)$$

Where E is an event in which the load is constant at a constant temperature. It can be generated from sampling the current signal at regular intervals of one hour. N_i is the number of events. W_E is the weight or severity associated with the event and Ah_E is the Ah throughput in the event E. Some particular values of temperature, SOC and C-rate must be considered as nominal values. When the Ah_{eff} of the battery becomes greater than the Ah throughput at the nominal operating conditions, then it can be considered as the end of life (EOL) of the battery [16].

3.4 Ageing Model

The capacity loss in a Li-ion battery is explained in (3.2) which is derived by conducting accelerated cycle life testing on the batteries. [24]

$$Q_{loss} = A \cdot \exp\left(\frac{-E_a}{R_{gas}T_k}\right) \cdot t^z \quad (3.2)$$

Where Q_{loss} is the percentage capacity loss, E_a is the activation energy ($Jmol^{-1}$), T_k is the temperature in kelvin, t is the cycling time. A is the pre-exponential factor, R_{gas} is the universal gas constant and z is the power law factor. In the ageing model defined in [25], Ah-throughput is used instead of time as it is proportional to time but the effect of SOC is neglected. In [26], an ageing model is defined in which the effect of both SOC and C-rate is considered (3.3).

$$Q_{cyc} = (\alpha SOC + \beta) \cdot \exp\left(\frac{-E_a + \eta \cdot C_{rate}}{R_{gas}T_k}\right) \cdot Ah^z \quad (3.3)$$

In this equation, Q_{cyc} is the capacity loss of the battery in percentage, α and β are the coefficients determined by curve fitting the experimental data and η is the C-rate compensation factor. The parameters of the ageing model are given in table 3.1 which are determined by fitting experimental data into (3.3).

Table 3.3 Values Of Parameters in (3.3)

Parameter	Value	
Fitting constant α	2896.6	$soc \leq 0.45$
	2694.5	$soc > 0.45$
Fitting constant β	7411.2	$soc \leq 0.45$
	6022.2	$soc > 0.45$
Compensation factor η	152.2	
Activation energy E_a	31500 J/mol	
Gas constant R_{gas}	8.314	
Power law factor z	0.57	

3.5 Severity Factor

In order to characterize the ageing of the battery under actual cycling conditions, severity factor is defined. The severity factor σ is the ratio of total charge throughput under nominal conditions to the total charge throughput under actual cycling conditions (3.4).

$$\sigma(t) = \frac{Ah_{nom}(SOC_{nom}, C_{rate,nom}, T_{k,nom})}{Ah_{cyc}(SOC, C_{rate}, T_k)} \quad (3.4)$$

Here Ah_{nom} is the total Ah throughput of the battery until its EOL when operated under nominal operating conditions given by as $SOC_{nom} = 0.35$, $T_{k,nom} = 298.15$ K and $C_{rate,nom} = 1C$. Ah_{cyc} is the total Ah throughput of the battery under the values at which the battery is actually operated. The values of Ah_{nom} is and Ah_{cyc} can be found using (3.3) as shown in (3.5) and (3.6).

$$Ah_{nom} = \left[\frac{Q_{cyc,EOL}}{(\alpha SOC_{nom} + \beta) \cdot \exp\left(\frac{-E_a + \eta \cdot C_{rate,nom}}{R_{gas}T_{k,nom}}\right)} \right]^{1/z} \quad (3.5)$$

$$Ah_{cyc} = \left[\frac{Q_{cyc,EOL}}{(\alpha SOC + \beta) \cdot \exp\left(\frac{-E_a + \eta \cdot C_{rate}}{R_{gas}T_k}\right)} \right]^{1/z} \quad (3.6)$$

When the maximum capacity delivered by the battery reduces to 20% if the initial capacity due to capacity fade, we consider that as end of life of the battery. Hence $Q_{cyc,EOL}$ is set as 20%.

The value of Ah_{nom} can be calculated by substituting the coefficients and values in (3.5). In [27], the value of Ah_{nom} is calculated for a 69 Ah battery using the coefficients in table 3.1. The capacity of BESS in our system is 540 Ah i.e. approximately eight 69 Ah batteries must be connected in

parallel to obtain this capacity. Hence in order to obtain the Ah_{nom} value for this battery pack, the Ah_{nom} which is calculated using (3.5) is multiplied with 8 and is obtained as **868935.83 Ah**.

3.6 Severity Factor Map

The effect of various factors on the severity factor can be observed by plotting the severity factor map. In this three dimensional plot, the variation of σ is plotted by keeping any one of the factors constant and varying other factors. The σ maps for different factors are plotted in figures 3.9 to 3.11.

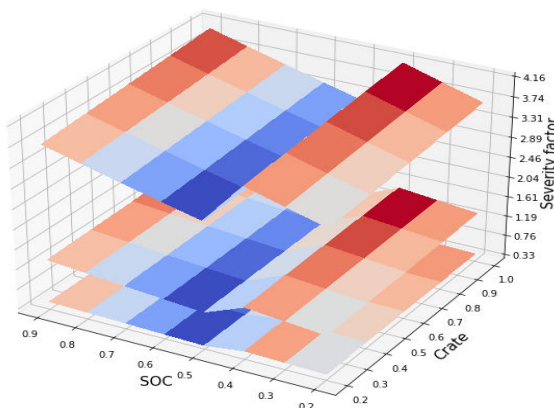


Figure 3.9Severity Factor Map at Temperatures 15 °C, 30 °C, 45 °C

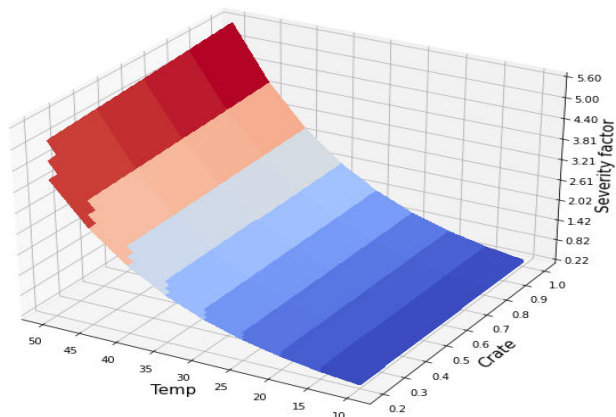


Figure 3.10Severity Factor Map at State of Charges 0.5, 0.7, 0.9

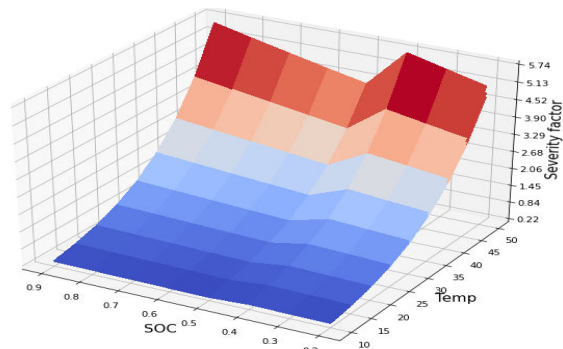


Figure 3.11Severity Factor Map at C-rates C, C/2, C/5

From the above plots, it is clear that the severity factor is mostly effected by temperature and is less effected by SOC and C-rate.

3.7 Expression for Degradation Cost of Battery

The severity factor can be used to find the value of Ah_{eff} as shown in (3.7).

$$Ah_{eff} = \sum_{k=1}^{N_i} \sigma(k) \cdot |I_{bat}(k)| \cdot \Delta t \tag{3.7}$$

Where I_{bat} is the battery current and N_i is the number of hours.

The concept of effective Ah throughput of the battery can be used for forming an expression for degradation cost or running cost C_{bd} of the battery in rupees as shown in (3.8). Here C_{bat} is the initial cost of the battery in rupees.

$$C_{bd} = \sum_{k=1}^{N_i} C_{bat} \cdot \frac{\sigma(k) \cdot |I_{bat}(k)|}{Ah_{nom}} \cdot \Delta t \tag{3.8}$$

This expression will be used as an objective function to minimise the running cost of the battery in order to increase its useful life. This expression can also be used to find the overall running cost of the system by adding the grid cost.

4. RESULTS

In this chapter, the optimization problem is solved using the methods explained in the previous chapter. The battery degradation cost and grid cost are evaluated and these values are compared to those of unoptimized case. The method giving minimum cost is determined and the plots of fitness function and battery and grid powers for each algorithm are shown.

4.1 Evaluation of the Costs

For solving the optimization problem the forecasted data of PV and load power for one month duration is considered. The grid cost is evaluated using the tariff rates given below in table 4.1 [32].

Table 5.1 Tariff rates for calculating grid cost

Cate gory	Energy (Rs/unit)	charge
0-100	3.44	
101-300	7.34	
301-500	10.36	
501-1000	11.82	

In addition to above costs, there will be a fixed cost of Rs. 102 per connection. As the system consists of three prosumers, it is assumed that the total energy consumed is divided into three equal parts. The grid cost of one connection is evaluated and it is multiplied by 3 to get total grid cost. The battery degradation cost which is evaluated after the optimization is added to the grid cost to get overall running cost of the system. The costs evaluated for different techniques are given in table 4.2.

Table 4.2 Degradation and Grid Costs for Different Optimization Techniques

	Unopt imized	AB C	PS O	G WO	T LBO
C_{bd}	5056.3	428	447	463	48

(Rs)	8	1.88	3.39	2.16	79.1
Grid consumption (KWH)	322.74	322.26	322.26	322.26	32.26
C_{grid} (Rs)	6449.0	643.39	643.39	643.39	64.339
Overall running cost (Rs)	11505.4	107.1578	109.0729	110.6605	11.313

From the above results it is clear that degradation cost (C_{bd}) is less for optimized case when compared to unoptimized case. Among the optimization algorithms, artificial bee colony optimization showed minimum value for C_{bd} . The grid cost is same for all the optimization algorithms and it is almost equal to unoptimized case. In case of overall running cost also, ABC algorithm gave minimum cost.

4.2 Plots of Battery and Grid Powers and Fitness Function

The plots of battery and grid powers for all the cases are given in figures (5.3) to (5.6). The variation of fitness function with number of iterations for different optimization techniques are also shown in figures (5.7) to (5.10). It can be seen that ABC algorithm took more number of iterations to converge to a minimum value. But as this is an offline study, number of iterations need not be considered as a criteria for an algorithm.

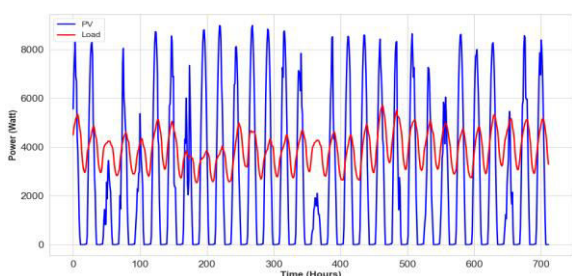


Figure 4.1 Forecasted Value of PV and Load Powers for One Month Duration

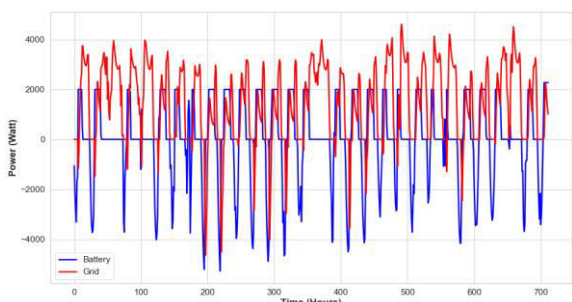


Figure 4.2 Variations in Battery and Grid Powers in Unoptimized Case

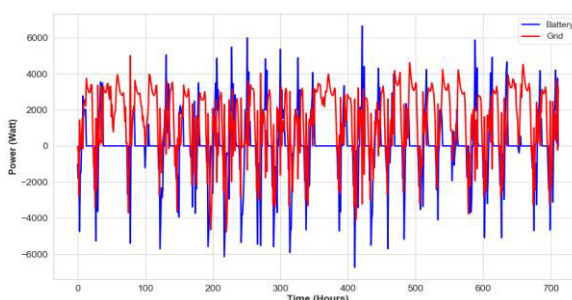


Figure 4.3 Variations in Battery and Grid Powers in ABC Algorithm

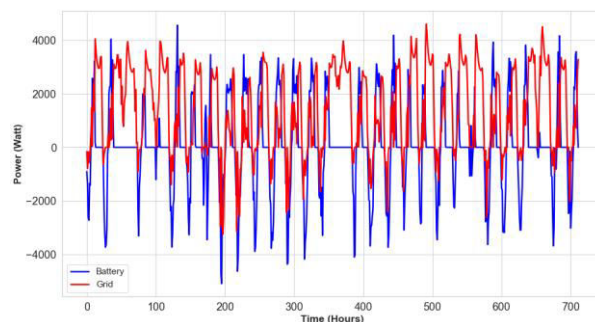


Figure 4.4 Variations in Battery and Grid Powers in PSO Algorithm

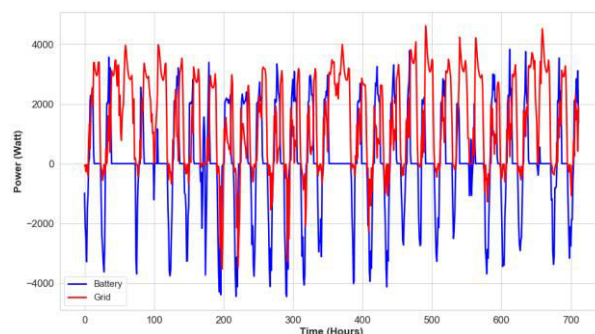


Figure 4.5 Variations in Battery and Grid Powers in GWO Algorithm

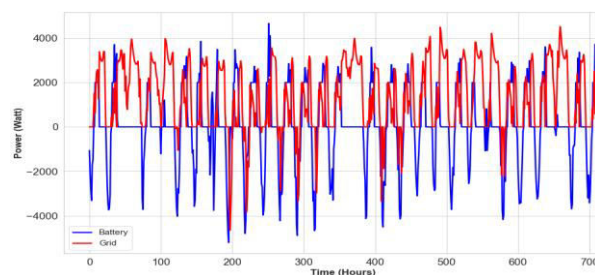


Figure 4.6 Variations in Battery and Grid Powers in TLBO Algorithm

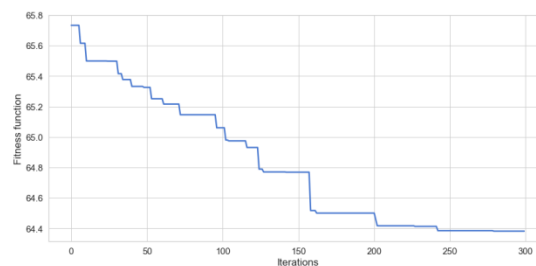


Figure 4.7 Variation of Fitness Function with Iterations in ABC Algorithm

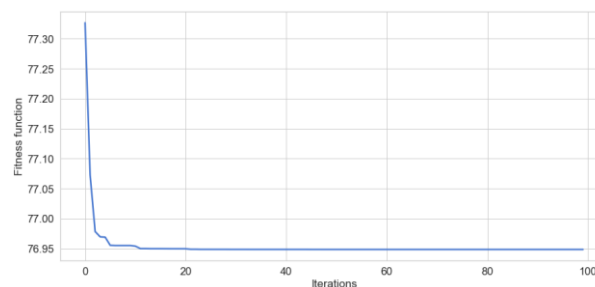


Figure 4.8 Variation of Fitness Function with Iterations in PSO Algorithm

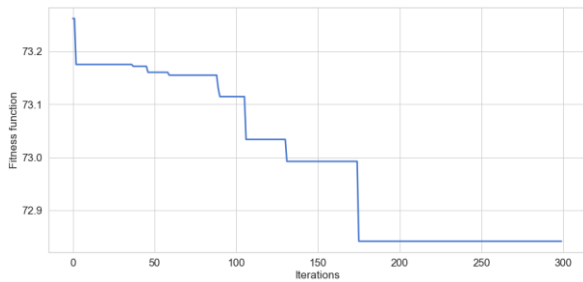


Figure 4.9 Variation of Fitness Function with Iterations in GWO Algorithm

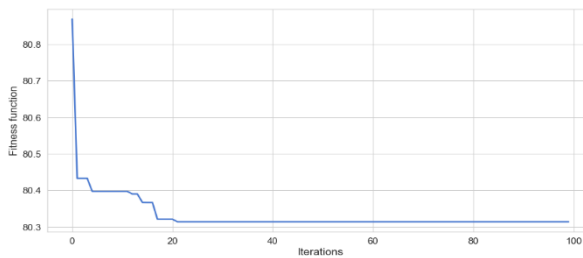


Figure 4.10 Variation of Fitness Function with Iterations in TLBO Algorithm

5. CONCLUSION AND FUTURE SCOPE

5.1 Conclusion

In this project, a grid connected rooftop PV system consisting of PV array, BESS and residential load is considered and the running cost of the BESS is reduced. As it is an offline optimization process, it requires the forecasted values of PV power and load power in order to schedule the battery power at each hour. Hence the historical datasets of insolation and load are utilised and forecasting is implemented using three machine learning algorithms and the algorithm giving accurate results is selected and is used for predictions. Among the three machine learning methods, LSTM network gave accurate predictions and is used for forecasting in further work.

The sizing of BESS in the system is done to meet the critical load demand for 12 hours in case of grid outage condition. Outages are created for different durations of time and the variations in SOC, battery power and grid power are plotted. A Li-ion battery ageing model which is affected by temperature, state of charge and C-rate is identified and the expression for degradation cost of Li-ion battery is derived.

The optimization problem is formulated along with the required constraints and it is solved using four metaheuristic techniques. The results of optimization are compared with that of operation without optimization. The forecasted data of one month is considered and above analysis is performed on it. Among all the algorithms artificial bee colony algorithm gave minimum value of degradation cost. The grid cost is evaluated and it is observed that it is almost same for unoptimised and optimised operation. Then the overall running cost for one month duration is also calculated by adding degradation cost and grid cost.

5.2 Future Scope

The battery degradation is also effected by climatic conditions. If the battery is installed in a place with a hotter weather its degradation is rapid. The study of battery

degradation can be done by considering different climatic conditions and they can be included in the ageing model so that the model will be more accurate.

The grid cost in this project is evaluated using static electricity tariff. But it can be evaluated by dynamic electricity tariff rate so that overall running cost of the system can be optimised. The concept of battery degradation can be applied to an electric vehicle battery as mostly Li-ion batteries are used. The load on the electric vehicle can be tracked and the battery's degradation can be minimised by framing an offline or an online optimization problem.

REFERENCES

- [1] Y. Riffonneau, S. Bacha, F. Barruel, and S. Ploix, "Optimal Power Flow Management for Grid Connected PV Systems With Batteries," *IEEE Trans. Sustain. Energy*, vol. 2, no. 3, pp. 309–320, Jul. 2011, doi: 10.1109/TSTE.2011.2114901.
- [2] M. Grids, "National Policy for Renewable Energy based Micro and Mini Grids," pp. 38–41, 2003.
- [3] G. of I. Ministry of Science & Technology, "Research, Development, Demonstration and Deployment of Smart Grids in India," 2017.
- [4] Harsha Kamak, Net metering Vs Gross metering, <https://solarify.in/blog/net-versus-gross-metering/>.
- [5] Ministry of Power, Rights to the electricity consumers through "Electricity (Right of consumers) rules", 2020. <https://pib.gov.in/PressReleasePage.aspx?PRID=1682384>
- [6] G. Albright, J. Edie, and S. Al-Hallaj, "A Comparison of Lead Acid to Lithium-ion in Stationary Storage Applications Contributors:," *AllCell Technol. LLC*, no. March, p. 14, 2012.
- [7] Y.-Y. Hong, J. J. F. Martinez, and A. C. Fajardo, "Day-Ahead Solar Irradiation Forecasting Utilizing Gramian Angular Field and Convolutional Long Short-Term Memory," *IEEE Access*, vol. 8, pp. 18741–18753, 2020, doi: 10.1109/ACCESS.2020.2967900.
- [8] T. M. Mitchell, "Machine learning. 1997," *Burr Ridge, McGraw Hill*, vol. 45, no. 37, pp. 870–877, 1997.
- [9] H. S. Hippert, C. E. Pedreira, and R. C. Souza, "Neural networks for short-term load forecasting: A review and evaluation," *IEEE Trans. Power Syst.*, vol. 16, no. 1, pp. 44–55, 2001, doi: 10.1109/59.910780.
- [10] H. Chen, C. A. Cañizares, and A. Singh, "ANN-based short-term load forecasting in electricity markets," in *Proceedings of the IEEE Power Engineering Society Transmission and Distribution Conference*, 2001, vol. 2, no. WINTER MEETING, pp. 411–415, doi: 10.1109/PESW.2001.916876.
- [11] A. G. Bakirtzis, V. Petridis, S. J. Klartzis, M. C. Alexiadis, and A. H. Maissis, "A neural network short term load forecasting model for the greek power system," *IEEE Trans. Power Syst.*, vol. 11, no. 2, pp. 858–863, May 1996, doi: 10.1109/59.496166.

- [12] M. O. Badawy, F. Cingoz, and Y. Sozer, "Battery storage sizing for a grid tied PV system based on operating cost minimization," in *ECCE 2016 - IEEE Energy Conversion Congress and Exposition, Proceedings*, 2016, pp. 1–7, doi: 10.1109/ECCE.2016.7854896.
- [13] M. O. Badawy and Y. Sozer, "Power Flow Management of a Grid Tied PV-Battery System for Electric Vehicles Charging," *IEEE Trans. Ind. Appl.*, vol. 53, no. 2, pp. 1347–1357, 2017, doi: 10.1109/TIA.2016.2633526.
- [14] M. Fatnani, D. Naware, and A. Mitra, "Design of Solar PV Based EV Charging Station with Optimized Battery Energy Storage System," in *2020 IEEE First International Conference on Smart Technologies for Power, Energy and Control (STPEC)*, 2020, pp. 1–5, doi: 10.1109/STPEC49749.2020.9297719.
- [15] J. Wang *et al.*, "Cycle-life model for graphite-LiFePO₄ cells," *J. Power Sources*, vol. 196, no. 8, pp. 3942–3948, Apr. 2011, doi: 10.1016/j.jpowsour.2010.11.134.
- [16] S. Onori, P. Spagnol, V. Marano, Y. Guezennec, and G. Rizzoni, "A new life estimation method for lithium-ion batteries in plug-in hybrid electric vehicles applications," *Int. J. Power Electron.*, vol. 4, no. 3, p. 302, 2012, doi: 10.1504/IJPELEC.2012.046609.
- [17] S. Han, S. Han, and H. Aki, "A practical battery wear model for electric vehicle charging applications," *Appl. Energy*, vol. 113, pp. 1100–1108, Jan. 2014, doi: 10.1016/j.apenergy.2013.08.062.
- [18] R. Mulla, "Hourly Energy Consumption: Over 10 years of hourly energy consumption data from PJM in Megawatts," *Kaggle*, 2017. [Online]. Available: <https://www.kaggle.com/robikscube/hourly-energy-consumption>.
- [19] Andrey, "Solar Radiation Prediction: Task from NASA Hackathon," *Kaggle*, 2016. [Online]. Available: <https://www.kaggle.com/dronio/SolarEnergy>.
- [20] Aurélien Géron, "Hands on Machine learning with scikit learn and tensorflow", First edition, March 2017.
- [21] "Introduction to the Keras tuner", https://www.tensorflow.org/tutorials/keras/keras_tuner.
- [22] Jignesh Parmar, <https://electricalnotes.wordpress.com/2011/10/31/demand-factor-diversity-factor-utilization-factor-load-factor/>. Last referred 10, June, 2021.
- [23] "Demystifying India's rooftop policies", <https://www.ceew.in/sites/default/files/demystifying-india-rooftop-solar-policies.pdf>.
- [24] I. Bloom, B.W. Cole, J.J. Sohn, S.A. Jones, E.G. Polzin, V.S. Battaglia, G.L. Henriksen, C. Motloch, R. Richardson, T. Unkelhaeuser, D. Ingersoll, H.L. Case, "An accelerated calendar and cycle life study of Li ion cells," *J. Power Sources* 101 (2001) 238.
- [25] J. Wang *et al.*, "Cycle-life model for graphite-LiFePO₄ cells," *J. Power Sources*, vol. 196, no. 8, pp. 3942–3948, Apr. 2011, doi: 10.1016/j.jpowsour.2010.11.134.
- [26] G. Suri and S. Onori, "A control-oriented cycle-life model for hybrid electric vehicle lithium-ion batteries," *Energy*, vol. 96, pp. 644–653, Feb. 2016, doi: 10.1016/j.energy.2015.11.075.
- [27] S. Zhang, X. Hu, S. Xie, Z. Song, L. Hu, and C. Hou, "Adaptively coordinated optimization of battery ageing and energy management in plug-in hybrid electric buses," *Appl. Energy*, vol. 256, no. May, p. 113891, Dec. 2019, doi: 10.1016/j.apenergy.2019.113891.
- [28] J. Kennedy and R. Eberhart, "Particle swarm optimization," *Proceedings of ICNN'95 - International Conference on Neural Networks*, 1995, pp. 1942–1948 vol.4, doi: 10.1109/ICNN.1995.488968.
- [29] Karaboga D., Basturk B. (2007) Artificial Bee Colony (ABC) Optimization Algorithm for Solving Constrained Optimization Problems. In: Melin P., Castillo O., Aguilar L.T., Kacprzyk J., Pedrycz W. (eds) *Foundations of Fuzzy Logic and Soft Computing. IFSA 2007. Lecture Notes in Computer Science*, vol 4529. Springer, Berlin, Heidelberg.
- [30] R.V. Rao, V.J. Savsani, D.P. Vakharia, "Teaching-learning-based optimization: A novel method for constrained mechanical design optimization problems," *Computer-Aided Design*, Volume 43, Issue 3, 2011.